Available online at www.sciencedirect.com
SCIENCE DIRECT®
International Journal of Heat and Mass Transfer 47 (2004) 987–999
International Journal of HEAT and MASS TRANSFER
www.elsevier.com/locate/ijhmt

# The effect of viscous dissipation in thermally fully-developed electro-osmotic heat transfer in microchannels

D. Maynes, B.W. Webb *

*Department of Mechanical Engineering, Brigham Young University, 435 CTB, Provo, UT 84602, USA*

Received 7 March 2003; received in revised form 7 August 2003

**Abstract**

The influence of viscous dissipation on thermally fully-developed, electro-osmotically generated flow has been analyzed for a parallel plate microchannel and circular microtube under imposed constant wall heat flux and constant wall temperature boundary conditions. Such a flow is established not by an imposed pressure gradient, but by a voltage potential gradient along the length of the tube. The result is a combination of unique electro-osmotic velocity profiles and volumetric heating in the fluid due to the imposed voltage gradient. For large ratio of the microtube radius (or microchannel half-width) to Debye length, the wall-normal fluid velocity gradients can be extremely high, which has the potential for significant viscous heating. The solution for the fully-developed, dimensionless temperature profile and corresponding Nusselt number have been determined for both geometries and for both thermal boundary conditions. It is shown that three dimensionless parameters govern the thermal transport: the relative duct radius (ratio of the duct radius or plate gap half-width to Debye length), the dimensionless volumetric source (ratio of Joule heating to wall heat flux), and a dimensionless parameter that relates the magnitude of the viscous heating to the Joule heating. Surprisingly, it is shown that the influence of viscous dissipation is only important at low values of the relative duct radius. For magnitudes of the dimensionless parameters which characterize most practical electro-osmotic flow applications, the effect of viscous dissipation is negligible.


## 1. Introduction

Fluid transport in channels of hydraulic diameter of order 100 μm has found importance in a number of emerging technologies in micropower generation, thermal control of electronic devices, cell analysis and other biomedical diagnostic techniques. At these physical scales, generating fluid motion in the tube presents challenges. Pressure-driven flow technology requires significant pressures, and while micropumps exist suitable for use at such pressures [1–3], they are difficult to manufacture and maintain [1], and lack the precise control that is often needed in microfluidic applications [4]. Electro-osmotic flow generation has been suggested as a viable alternative to pressure-driven liquid flow at the microscale, with better flow control and no moving parts. Several investigators have reported on electro-osmotic pump systems [5–9]. Capillary electrophoresis is a chemical separations technique that utilizes electro-osmotically driven flows [10].

Electro-osmosis is the bulk movement of liquid relative to a stationary surface due to an externally applied electric field, and was first observed and reported by Reuss nearly two centuries ago [11]. Most solid substances will acquire a relative electric charge when in contact with an aqueous electrolytic solution, which in turn, influences the charge distribution in the solution. Ions of opposite charge (counterions) to that of the surface are attracted towards the surface and ions of the same charge (coions) are repelled from the surface as shown in Fig. 1a. The net effect is the formation of a region close to the charged surface called the electric double layer (EDL) in which there is an excess of counterions over coions, and which are distributed in a diffuse manner [12]. The charge distribution in the fluid therefore

* Corresponding author. Tel.: +1-801-422-6543; fax: +1-801-422-0156.
*E-mail address:* webb@byu.edu (B.W. Webb).

0017-9310/$ - see front matter © 2003 Elsevier Ltd. All rights reserved.
doi:10.1016/j.ijheatmasstransfer.2003.08.016

**Nomenclature**

| | |
|---|---|
| $a$ | tube radius or channel gap half-width |
| $C$ | fluid specific heat |
| $D_h$ | channel hydraulic diameter |
| $E_e$ | total Joule heating per channel length |
| $E_v$ | total viscous heating per channel length |
| $i_e$ | conduction current density |
| $k$ | thermal conductivity |
| $k_b$ | Boltzmann constant |
| $Nu$ | Nusselt number, $hD_h/k$ |
| $r$ | radial coordinate |
| $R$ | normalized radial coordinate, $r/a$ |
| $q''_w$ | wall heat flux |
| $s_e$ | volumetric Joule heating |
| $S$ | dimensionless Joule heating parameter, $s_e a/q''_w$ |
| $S_v$ | dimensionless viscous heating parameter, $\mu u_{eo}^2/s_e\lambda^2$ |
| $T$ | absolute temperature |
| $T_m$ | mixed mean temperature |
| $T_w$ | channel wall temperature |
| $u$ | local fluid velocity |
| $u_{eo}$ | maximum possible electro-osmotic velocity |
| $\bar{u}$ | average velocity |
| $U$ | normalized local velocity, $u/\bar{u}$ |
| $\overline{U}_{eo}$ | normalized average velocity, $\bar{u}/u_{eo}$ |
| $w$ | parallel plate channel width |
| $x$ | streamwise coordinate |
| $y$ | wall-normal coordinate |
| $Y$ | normalized wall-normal coordinate, $y/a$ |
| $Z$ | relative duct radius, $a/\lambda$ |

*Greek symbols*

| | |
|---|---|
| $\varepsilon$ | fluid dielectric constant |
| $\Phi$ | applied potential field |
| $\mu$ | fluid dynamic viscosity |
| $\mu_{eo}$ | electro-osmotic mobility |
| $\rho$ | fluid density |
| $\sigma$ | liquid electrical resistivity |
| $\theta$ | normalized temperature |
| $\theta_w$ | normalized wall temperature |
| $\lambda$ | Debye length |
| $\zeta$ | wall zeta potential |

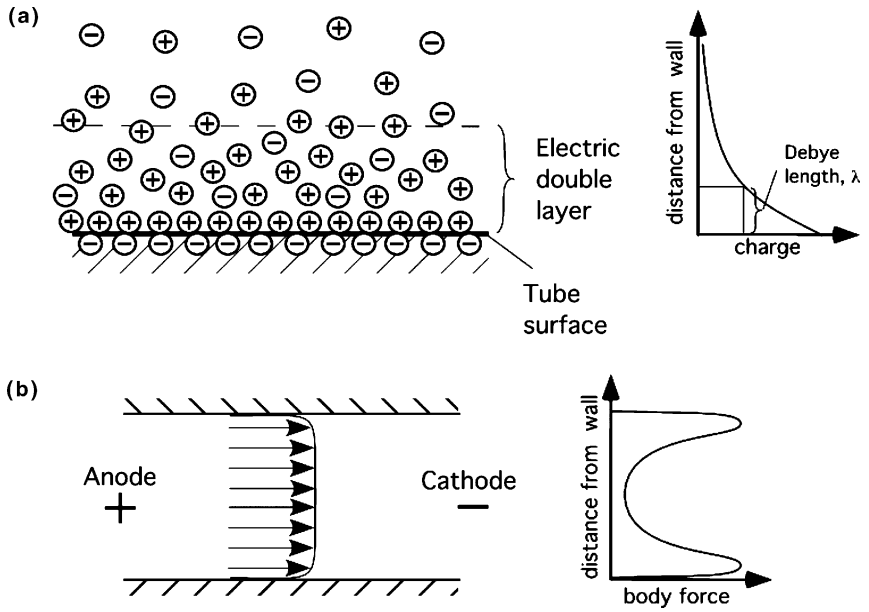


Fig. 1. Schematic illustration of electro-osmotically generated flow.

falls from its maximum near the wall (characterized by what is termed the zeta potential) to a zero charge in the fluid core (for large enough tube radius). The thickness of the EDL is characterized by the Debye length, which is the wall-normal distance over which the net charge has decreased from the charge magnitude near the tube surface to $1/e$ (37%) of the surface charge. As an example, glass and fused silica capillaries carry dissociable silanol groups on the surface, and are therefore negatively charged when adjacent to polar liquids. Other

weak electrolyte solutions also exhibit such characteristics. The positively charged cations and solvent molecules strongly adsorbed at the wall remain stationary under the influence of an electric potential in the streamwise direction, while the mobile cations in the EDL very near the tube walls will migrate toward the cathode due to the excess charge in the layer. This gives rise to a concentrated fluid body force near the tube walls as illustrated in Fig. 1b. Viscous shear forces transmitted from the EDL to the tube center pull the core fluid towards the cathode as well. The resulting electro-osmotic flow velocity distribution is a function of the ratio of the hydraulic radius to the Debye length. When the capillary radius is much larger than the Debye length, the resulting velocity profile exhibits a near-uniform distribution in the tube core, decreasing to the no-slip condition in a very thin fluid layer near the tube wall (layer thickness $< 1$ μm). At the other extreme, when the capillary radius is of the same order as the Debye length, the flow exhibits a maximum in velocity near the tube centerline gradually decreasing toward the wall, more nearly like that of classical pressure-driven flow. Of course, the total electro-osmotic flow rate in the tube is a function of the electro-osmotic characteristics of the tube/fluid combination (electro-osmotic mobility), tube radius (relative to Debye length), imposed voltage potential, fluid viscosity and permittivity, electrolyte concentration, etc. Generally speaking, the total induced flow rate is inversely related to the Debye length, viscosity, and electrolyte concentration, and is proportional to the imposed axial voltage gradient. At these physical scales and for some conditions, the resulting wall-normal gradients of axial velocity are extremely high—of order $10^4$–$10^5$ $s^{-1}$ for pure water in a 250 μm diameter microtube with an applied voltage gradient of 200 kV/m. It has long been suspected that the viscous heating resulting from such high velocity gradients can have a significant impact on the fluid temperature distribution.

The fluid dynamics of electro-osmotically generated flow are significantly different from traditional pressure-driven flow, and therefore, the thermal transport dynamics are expected to be quite different as well. The applied driving voltage gradient and its induced electric conduction current establishes Joule heating in the fluid, resulting in volumetric energy generation therein. The magnitude of the thermal energy source has significant influence on the temperature distribution and heat transfer. These phenomena, coupled with the viscous dissipation effects described in the foregoing paragraph, result in fully-developed thermal transport that is both interesting and complex. Even though the hydrodynamic development region for microchannels has been shown to be approximately four times longer than for traditional pressure-driven flow [13], a fully-developed condition is likely to prevail over the majority of the channel length.

Several analytical studies have appeared in the literature describing the hydrodynamics of fully-developed electro-osmotic flow through circular and rectangular channels. Specifically, several early papers report on electro-osmotic velocity distributions and the associated momentum transport in capillaries as a function of channel diameter-to-Debye length ratio [14–16]. More recent hydrodynamic studies have explored the effects on the velocity field due to streamwise gradients in the electrical conductivity [17], the transient response of the velocity field to a suddenly applied voltage gradient [18], the entry region flow field development [13,19], and effects of variations in the wall zeta potential on the velocity profile characteristics [20,21]. Additionally, some experimental studies have reported on the velocity profile characteristics associated with fully-developed electro-osmotic flow in very long circular and rectangular channels [22–27].

With regards to characterization of the convection heat transfer associated with electro-osmotic flow, relatively little prior work has appeared in the literature. Li and coworkers have explored electrokinetic effects induced in a pressure-driven flow on the frictional and heat transfer characteristics for both round and rectangular microchannels [28–30]. They report that the resulting induced electrokinetic potential results in a reduced flow rate, a greater friction factor, and a reduced Nusselt number from the classical laminar pressure-driven flow scenario. There also exists some early work exploring the effect of volumetric energy generation on thermal development in channels under pressure-driven flow conditions [31,32]. Other investigators have explored the influence of Joule heating on efficiency in capillary electrophoresis [33–36]. The fully-developed thermal transport for constant-property electro-osmotic flow in circular microtubes and parallel plate microchannels was previously explored for the case of negligible viscous heating [37]. The normalized temperature distributions and resulting Nusselt numbers were found to be a function of the microchannel relative radius (ratio of channel radius to Debye length) and dimensionless volumetric source (due to Joule heating). Additionally, thermally fully-developed heat transfer has been explored for combined electro-osmotic and pressure driven, constant-property flow in a circular microtube under imposed constant wall heat flux boundary condition [38]. Such a flow is established by the combination of an imposed pressure gradient and voltage potential gradient along the length of the tube. Possible scenarios include opposing and assisting pressure and voltage gradients.

No studies have appeared in the literature that specifically address the influence of viscous heating on the fluid temperature distributions and convective heat transport characteristics for purely electro-osmotically driven flow. This study presents solutions for thermally

fully-developed electro-osmotic flow in circular and parallel plate microchannels (based on previously reported velocity distributions) for both constant wall heat flux and constant wall temperature boundary conditions. Conditions for which viscous dissipation exercises influence on the temperature distribution are identified. The analysis assumes no pressure-driven component to the velocity field and constant fluid properties (electrical and thermal conductivity, viscosity, electro-osmotic mobility, etc.). Also, the wall zeta potential is assumed to be constant and less than $3k_bT$ such that the Debye–Hückel linearization holds [12]. The total electrical current drawn in electro-osmotically generated flow consists of two components, the so-called conduction and convection currents. Joule heating in the fluid arises from the conduction current only and may be safely modeled using Ohm's law [15]. Further, this energy generation is distributed uniformly across the tube or channel cross-section for low zeta potential (as imposed here) [16], whereas the viscous heating results in spatially non-uniform energy generation.

## 2. Hydrodynamic considerations

Consider fully-developed flow of an incompressible fluid in a microchannel (circular or rectangular of infinite width) with coordinates defined in Fig. 2, where the flow is driven electro-osmotically (in the absence of applied pressure gradient). For low wall potential, the Debye–Hückel linearization is valid [12], and the excess charge distribution may be expressed explicitly as a function only of the zeta potential, the Debye length $\lambda$, and the wall-normal coordinate $y$. For such a scenario, the momentum equation may be solved subject to boundary conditions reflecting no slip at the wall and zero shear stress at the centerline, yielding fully-developed electro-osmotic velocity distributions for the parallel plate and circular tube, respectively, as [12,14]

$$\frac{u}{u_{eo}} = 1 - YZe^{-Z} - e^{-YZ} \quad (Y \leqslant 1) \tag{1}$$

and

$$\frac{u}{u_{eo}} = 1 - \frac{I_0(ZR)}{I_0(Z)} \tag{2}$$

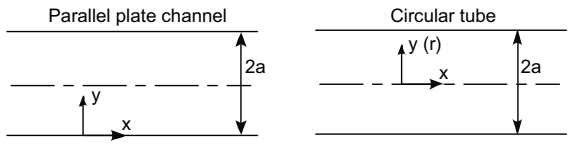


Fig. 2. Definition of coordinate system and dimensions for parallel plate channel and circular tube.

$Y$ ($= y/a$ for the parallel plate channel) or $R$ ($= r/a$ for the circular tube) is the non-dimensional wall-normal coordinate, $Z$ is the relative duct radius (ratio of tube radius or gap half-width to the Debye length, $a/\lambda$), and $I_0$ is the modified Bessel function of the first kind of order 0. The Debye length is a function of the electrochemical characteristics of the liquid/tube interface, and is rather difficult to measure. It may be estimated from the relation $\lambda = (\varepsilon RT/2F^2z^2c)^{1/2}$ where $\varepsilon$, $T$, $R$, and $F$ are the fluid permittivity, absolute temperature, universal gas constant, and Faraday's constant, respectively [12]. The parameters $z$ and $c$ are the valence number and average molar concentration of ions in the liquid solution. The expression reveals that the Debye length may vary nominally between 1 and 1000 nm. For large $Z$ the size of the electric double layer or region of excess charge (and corresponding source of fluid momentum) is relatively small. Conversely, for $Z < 1$ the double layer thickness is smaller than the channel radius and the region of excess charge (and source of fluid momentum) is approximately uniformly distributed over the entire channel. The term $u_{eo} = (\varepsilon\zeta/\mu)\mathrm{d}\Phi/\mathrm{d}x$ represents the maximum possible electro-osmotic velocity for a given applied potential field, where $\mu_{eo} = \varepsilon\zeta/\mu$ is often termed the electro-osmotic mobility of the liquid [39]. For large $Z$ ($Z > 500$) Eqs. (1) and (2) reduce to $u/u_{eo} = 1$ which is the classical Helmoltz–Smoluchowski equation [12].

Integration over the duct cross-sectional area yields the normalized average velocities expressed as

$$\frac{\bar{u}}{u_{eo}} = 1 - \frac{Ze^{-Z}}{2} + \frac{e^{-Z}}{Z} - \frac{1}{Z} \tag{3}$$

and

$$\frac{\bar{u}}{u_{eo}} = 1 - \frac{2I_1(Z)}{ZI_0(Z)} \tag{4}$$

for the two configurations, respectively. $I_1$ is the modified Bessel function of the first kind of order 1. Eqs. (3) and (4) show that for increasing $Z$ the average velocity increases toward the maximum electro-osmotic velocity, $u_{eo}$, for both configurations.

Profiles of the normalized local velocity, $u/u_{eo}$, are shown in Fig. 3 for the parallel plate and circular ducts for $Z$ varying between 0.3 and 300. These represent reasonable limits on $Z$ for practical electro-osmotic flow applications. As stated previously, the Debye length $\lambda$ is fixed by the electrochemical characteristic of the fluid-channel interface [12]. Large values of $Z$ arise when the Debye layer occupies a very small portion of the channel cross-section. Thus, for $Z \to \infty$, the velocity profiles shown in Fig. 3 exhibit slug-like behavior with a very thin boundary layer at the wall. Conversely, small values of $Z$ arise when the Debye layer is of the same

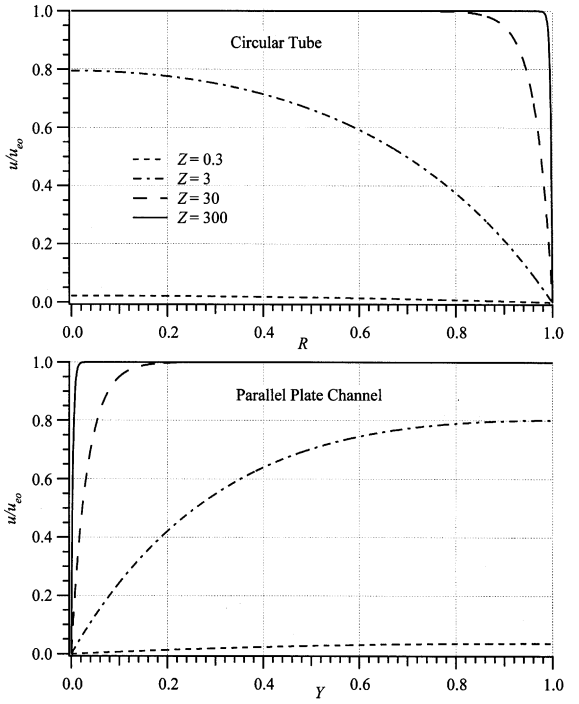


Fig. 3. Normalized electro-osmotic velocity distributions in a parallel plate channel and circular tube for $Z = 0.3$, 3, 30, and 300.

physical scale as the microchannel radius. The lower limit $Z = 0.3$ presented here reflects a reasonable lower limit, representative of electro-osmotic flow in nanochannels. Fig. 3 shows that as $Z$ vanishes, the profiles approximate the parabolic distributions of classical Poiseuille flow. For decreasing $Z$ the velocity magnitude decreases, consistent with the average velocity integrations of Eqs. (3) and (4). As the electric double layer penetrates the core fluid and the excess charge distribution is spread over a larger portion of the channel cross-section, the induced electro-osmotic velocity drops. At intermediate values of relative duct radius, where the source of momentum varies from a concentrated source near the duct walls (large $Z$) to a more uniformly distributed source (small $Z$) the velocity profiles change accordingly.

From Eqs. (1) and (2), the magnitude of the maximum velocity gradient, $|\mathrm{d}u/\mathrm{d}y|_{\mathrm{wall}}$, may be expressed as $(u_{\mathrm{eo}}/a)Z(1-\mathrm{e}^{-Z})$ and $(u_{\mathrm{eo}}/a)ZI_1(Z)/I_0(Z)$ for the parallel plate and circular tube microchannels, respectively. At large $Z$, the velocity gradient at the wall is thus proportional to $Z$ for both geometries. The implication is the existence of a region of extremely high wall-normal velocity gradient near the wall, which may result in significant viscous heating for large relative duct radius.

## 3. Thermal transport considerations

Considering steady hydrodynamically fully-developed flow with constant thermophysical properties, the energy equation simplifies to

$$k\frac{\partial^2 T}{\partial x^2}+\frac{k}{y^n}\frac{\partial}{\partial y}\left(y^n\frac{\partial T}{\partial y}\right)=\rho Cu\frac{\partial T}{\partial x}-s_{\mathrm{e}}-\mu\left(\frac{\mathrm{d}u}{\mathrm{d}y}\right)^2 \tag{5}$$

where $n = 0$ and 1 for the parallel plate channel and circular tube, respectively. The case of constant thermophysical properties represents a limiting case from which scenarios involving variable transport properties for specific fluids will deviate. $T$ is the local temperature and $s_{\mathrm{e}}$ is the volumetric generation due to the electrical resistance heating. The last term on the right-hand side of Eq. (5) is the local volumetric heating due to viscous dissipation, and is proportional to the square of the velocity gradient. The total current drawn under electro-osmotically generated flow is the sum of the so-called conduction and convection currents. The volumetric Joule heating $s_{\mathrm{e}}$ arises from the conduction current only, and may be accurately modeled using Ohm's law [15]. Further, for low zeta potential (as is considered here) or for large channel hydraulic diameter-to-Debye length ratios, this energy generation is uniformly distributed across the microchannel cross-section [16]. For electro-osmotically driven flow then, $s_{\mathrm{e}} = i_{\mathrm{e}}^2\sigma$ where $i_{\mathrm{e}}$ is the conduction current density ($\mathrm{A/m^2}$) and $\sigma$ is the liquid electrical resistivity ($\Omega\,\mathrm{m}$). For an applied potential gradient along the microchannel axis $\mathrm{d}\Phi/\mathrm{d}x$, the volumetric energy source due to Joule heating may thus be expressed as $s_{\mathrm{e}} = (\mathrm{d}\Phi/\mathrm{d}x)^2/\sigma$.

Before solving the energy equation, Eq. (5), subject to either imposed wall heat flux or imposed wall temperature boundary conditions, it is instructive to examine the relative magnitudes of total volumetric generation by viscous and Joule heating. The total energy generated by Joule heating per channel length is simply $E_{\mathrm{e}} = \pi s_{\mathrm{e}} a^2$ and $E_{\mathrm{e}} = s_{\mathrm{e}} a w$ for the circular tube and parallel plate channel ($w$ is the width of the channel), respectively. Determination of the total viscous heating requires integration of the dissipation term in the energy equation over the channel cross-section. For the circular tube, for example, this becomes

$$E_{\mathrm{v}} = \mu\int_0^a\left(\frac{\mathrm{d}u}{\mathrm{d}r}\right)^2 2\pi r\,\mathrm{d}r \tag{6}$$

Following integration of Eq. (6), the ratio of viscous to Joule heating for either channel geometry may be shown to be of the form

$$E_{\mathrm{v}}/E_{\mathrm{e}} = S_{\mathrm{v}}F(Z) \tag{7}$$

where the function $F(Z)$ is shown in Table 1. The dimensionless parameter $S_{\mathrm{v}}$ is a measure of the relative magnitudes of viscous and Joule heating, and is defined

Table 1
Expressions for the functions $F(Z)$ and $G(Y,Z)$ in Eqs. (7) and (10)

*Parallel plate channel:*

$$F(Z) = \frac{3e^{-2Z}}{2Z} - \frac{2e^{-Z}}{Z} + e^{-2Z} + \frac{1}{2Z}$$

$$G(Y,Z) = e^{-2ZY} + e^{-2Z} - 2e^{-Z(Y+1)}$$

*Circular tube (for $Y = R$):*

$$F(Z) = \frac{I_1^2(Z)}{I_0^2(Z)} + \frac{2}{Z}\frac{I_1(Z)}{I_0(Z)} - 1$$

$$G(R,Z) = \frac{I_1^2(ZR)}{I_0^2(Z)}$$

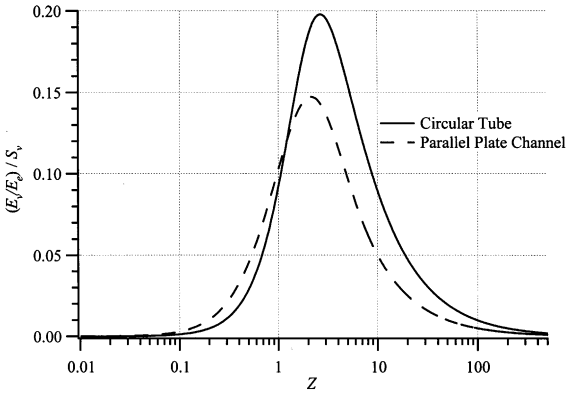


Fig. 4. Ratio of viscous to Joule heating $(E_v/E_e)/S_v$ plotted vs. $Z$ for the circular tube and parallel plate channel.

as $S_v = \mu u_{eo}^2/s_e\lambda^2$. Since the maximum electro-osmotic velocity is given by $u_{eo} = \mu_{eo}(d\Phi/dx)$, and the volumetric Joule heating has been previously shown to be of magnitude $s_e = (d\Phi/dx)^2/\sigma$, this parameter may be expressed in terms of more fundamental parameters as $S_v = \sigma\mu\mu_{eo}^2/\lambda^2$. $S_v$ is therefore dependent only on physical and electro-osmotic properties of the fluid. It is useful to characterize the range of $S_v$ which might be encountered in practical electro-osmotic flow applications. The electrical resistivity, $\sigma$, varies inversely with electrolyte concentration [12], and the Debye length, $\lambda$, varies inversely with the square root of concentration [12]. Thus, their net effect on $S_v$ cancels. Consequently, $S_v$ varies as the square of the electro-osmotic mobility, which has been observed to decrease with increasing electrolyte concentration [10,40]. For the range of parameters reported in the literature, $S_v$ may assume values with a maximum of the order of 10 [7,10,40]. Values of $S_v$ may be estimated for specific electro-osmotic flow applications by measuring combinations of the potential gradient, electrolyte concentration, conduction current, and induced flow rate. The Debye length is determined from the measured electrolyte concentration and valence number, and fluid temperature [12].

Eq. (7) reveals that the ratio of viscous heating to Joule heating in an electro-osmotic flow is proportional to the dimensionless viscous heating parameter $S_v$. Fig. 4 shows this ratio divided by $S_v$ as a function of $Z$ for both the circular tube and the parallel plate channel. At the extremes of the relative radius $Z$, the viscous heating becomes negligible in comparison with the Joule heating. However, at an intermediate value of $Z$ the viscous dissipation/Joule heating ratio exhibits a maximum. This occurs at $Z \approx 2.5$ and 3, respectively, for the parallel plate channel and circular tube. It is also interesting to note that with peak magnitudes of $(E_v/E_e)/S_v$ of 0.15–0.2, and for typical magnitudes of $S_v$ of O(10) or less, the viscous heating may be as much as 150–200% of the total volumetric energy generation in the channel, but is more likely a fraction less than 1. The maximum in the $(E_v/E_e)/S_v$ vs. $Z$ behavior may be explained as follows. At high relative duct radius the wall-normal velocity gradients are high, but confined to a very small spatial region near the channel wall. As $Z$ decreases in magnitude the velocity gradients also decrease, but the spatial region affected by the resulting viscous heating increases more rapidly. At the extreme low values of $Z$ the magnitude of the velocity gradient nearly vanishes, both because of reduced velocity magnitude and a profile with small velocity gradients. The maximum in $(E_v/E_e)/S_v$ at $Z \approx 2.5$ represents the scenario where the velocity gradient is significant over much of the tube cross-section. Given that the magnitude of the Debye length is nominally 10–500 nm, the implication for practical electro-osmotic flow situations is that viscous heating will contribute significantly to the total temperature rise of the fluid only in nanoscale channels.

The case of thermally fully-developed flow is defined classically by the condition

$$\frac{\partial}{\partial x}\left(\frac{T_w - T}{T_w - T_m}\right) = 0 \tag{8}$$

This condition and the resulting implications on the thermal transport are now treated for both the constant wall heat flux and constant wall temperature boundary conditions.

## 4. Constant wall heat flux

For an imposed constant heat flux boundary condition ($q''_w = \text{constant}$), the thermally fully-developed condition of Eq. (8) yields $\partial T/\partial x = dT_m/dx = \text{constant}$ and $\partial^2 T/\partial x^2 = 0$. Furthermore, an energy balance on the fluid yields

$$\rho\bar{u}C\frac{\mathrm{d}T_\mathrm{m}}{\mathrm{d}x}=\frac{4q''_\mathrm{w}}{D_\mathrm{h}}+s_\mathrm{e}+\frac{2^{n+2}\mu}{D_\mathrm{h}^{n+1}}\int_0^a\left(\frac{\mathrm{d}u}{\mathrm{d}y}\right)^2 y^n\,\mathrm{d}y \tag{9}$$

In the equation above, $D_\mathrm{h}$ is the hydraulic diameter. Again, $n=0$ and 1 for the parallel plate microchannel and circular microtube, respectively. Substituting Eq. (9) into Eq. (5) and introducing a normalized temperature $\theta=(T-T_\mathrm{m})/(q''_\mathrm{w}a/k)$, yields the non-dimensional energy equation

$$U\{2^n+S[1+S_\mathrm{v}F(Z)]\}=\frac{1}{Y^n}\frac{\mathrm{d}}{\mathrm{d}Y}\left(Y^n\frac{\mathrm{d}\theta}{\partial Y}\right)+S[1+S_\mathrm{v}G(Y,Z)] \tag{10}$$

where $U=u/\bar{u}$, $S=s_\mathrm{e}a/q''_\mathrm{w}$, and $S_\mathrm{v}$ is as previously defined. The dimensionless parameter $S$ represents the magnitude of Joule heating compared with the imposed wall heat flux. The function $F(Z)$ is identical to that which appeared in Eq. (7) and was presented in Table 1. The dimensionless parameter $G(Y,Z)$ is also included in Table 1 for the parallel plate channel and circular tube. The boundary conditions associated with the energy equation are $\mathrm{d}\theta/\mathrm{d}Y=\pm1$ at the wall (with the sign chosen appropriate to each geometry), and $\mathrm{d}\theta/\mathrm{d}Y=0$ at the centerline. In practice, one may impose an as-yet-undetermined wall temperature $\theta_\mathrm{w}=(T_\mathrm{w}-T_\mathrm{m})/(q''_\mathrm{w}a/k)$, and the solution of Eq. (10) results in an expression for $\theta$ in terms of $\theta_\mathrm{w}$. The unknown wall temperature $\theta_\mathrm{w}$ is then found by evaluating the normalized mixed mean temperature from its definition:

$$\int_0^1 U(Z,Y)\theta(Z,Y)Y^n\,\mathrm{d}Y=0 \tag{11}$$

Substituting the normalized velocity $U(Y,Z)$ for electro-osmotic flow, and the functions $F(Z)$ and $G(Y,Z)$ in Eq. (10), and integrating twice yields the following general expression for the temperature distribution

$$\theta-\theta_\mathrm{w}=\frac{2^n+S[1+S_\mathrm{v}F(Z)]}{\overline{U}_\mathrm{eo}}A_2(Y,Z)+S[A_1(Y)-S_\mathrm{v}A_3(Y,Z)] \tag{12}$$

where the functions $A_1(Y)$, $A_2(Y,Z)$, and $A_3(Y,Z)$ are shown in Table 2 for both channel configurations. Note that the product $SS_\mathrm{v}$ describes the relative magnitudes of viscous heating and the imposed wall heat flux.

The fully-developed Nusselt number may be expressed generally as

$$Nu=\frac{q''_\mathrm{w}D_\mathrm{h}}{k(T_\mathrm{w}-T_\mathrm{m})}=\frac{D_\mathrm{h}}{a}\frac{1}{\theta_\mathrm{w}} \tag{13}$$

and can thus be determined in terms of $S$, $S_\mathrm{v}$, and $Z$ from the wall temperature $\theta_\mathrm{w}$. In practice, Eq. (11) was integrated numerically to determine $\theta_\mathrm{w}$ using the trapezoidal rule for a specified $S$, $S_\mathrm{v}$, and $Z$ using a spatial interval $\Delta Y(\Delta R)=0.001$. The accuracy of the numerical integration was validated to better than 1% by comparison with several classical solutions for no volumetric Joule and no viscous heating: (1) for a Poiseuille (parabolic) flow velocity profile, $Nu=8.23$ and 4.36 for the parallel plate channel and circular tube, respectively [41]; and (2) electro-osmotic flow approaching a slug-flow condition as $Z\to\infty$, $Nu=12$ and 8, respectively, for the two geometries [41]. The Nusselt number dependence on $S$, $S_\mathrm{v}$,

Table 2
Expressions for the functions $A_1(Y)$, $A_2(Y,Z)$, and $A_3(Y,Z)$ in the solution for dimensionless temperature, Eq. (12)

*Parallel plate channel:*

$$A_1(Y)=-\left(\frac{Y^2}{2}-Y\right)$$

$$A_2(Y,Z)=\frac{1}{Z^2}(1-\mathrm{e}^{-YZ})-Y\left(1+\frac{\mathrm{e}^{-Z}}{Z}-\frac{Z\mathrm{e}^{-Z}}{2}\right)+\frac{Y^2}{2}-\frac{Y^3}{6}Z\mathrm{e}^{-Z}$$

$$A_3(Y,Z)=\frac{1}{Z^2}\left[\frac{1}{4}(\mathrm{e}^{-2YZ}-1)+2(\mathrm{e}^{-Z}-\mathrm{e}^{-Z(Y+1)})\right]-Y\left(\mathrm{e}^{-2Z}+\frac{3\mathrm{e}^{-2Z}}{2Z}\right)$$

*Circular tube (for $Y=R$):*

$$A_1(R)=-\tfrac{1}{4}(R^2-1)$$

$$A_2(R,Z)=\frac{1}{Z^2}\left[1-\frac{I_0(RZ)}{I_0(Z)}\right]+\frac{1}{4}(R^2-1)$$

$$A_3(R,Z)=\frac{1}{2}\left[1-\frac{I_1^2(Z)}{I_0^2(Z)}\right]+\frac{1}{2Z}\left[R\frac{I_1(RZ)I_0(RZ)}{I_0^2(Z)}-\frac{I_1(Z)}{I_0(Z)}\right]+\frac{1}{2Z^2}\left[\frac{I_0^2(RZ)}{I_0^2(Z)}-1\right]-\frac{R^2}{2}\left[\frac{I_0^2(RZ)}{I_0^2(Z)}-\frac{I_1^2(RZ)}{I_0^2(Z)}\right]$$

and $Z$ will be explored over their full ranges in the sections to follow.

Previously, the range of the dimensionless viscous heating parameter which might be encountered in typical electro-osmotically generated flow was characterized. It is important to explore the practical range of $S$ for such a flow as well. Substituting the expression for $s_e$, the dimensionless Joule heating parameter becomes $S = i_e^2 \sigma a / q''_w$. Thus, the applicable extremes for this parameter are $S \to 0$ for vanishing Joule heating and/or large imposed wall heat flux, and $S \to \infty$ for insulated microchannel conditions approaching an adiabatic boundary. Thus $S$ may realistically take on any positive, finite value (assuming only positive values of $q''_w$ consistent with practical fluid heating conditions), although very large values of $S$ are unlikely in realistic applications.

Figs. 5 and 6 plot the fully-developed Nusselt numbers as a function of $S_v$ for four values of the relative duct radius $Z$, and $S$ ranging from 0.1 to 100 for the

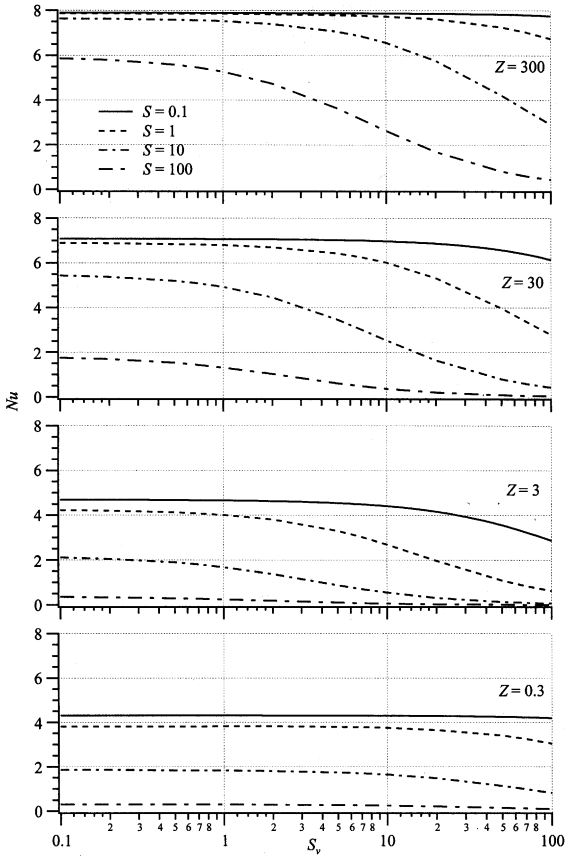


Fig. 5. Fully-developed Nusselt number in the circular channel with an imposed constant heat flux (fluid heating) plotted vs. the viscous heating parameter, $S_v$, for $Z = 0.3$, 3, 30, and 300, and $S = 0.1$, 1, 10, and 100.

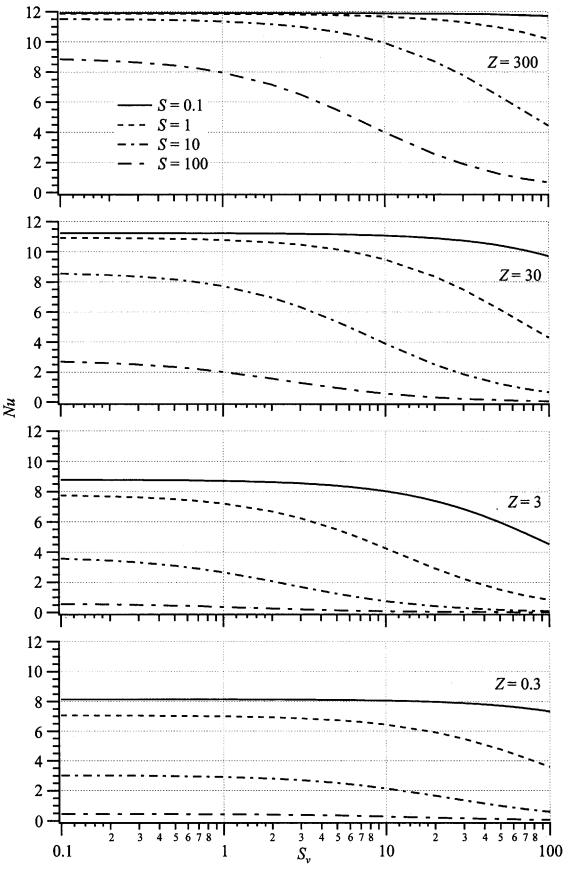


Fig. 6. Fully-developed Nusselt number in the parallel plate channel with an imposed constant heat flux (fluid heating) plotted vs. the viscous heating parameter, $S_v$, for $Z = 0.3$, 3, 30, and 300, and $S = 0.1$, 1, 10, and 100.

circular tube and parallel plate channel, respectively. Note that the Nusselt number behavior is shown for values of $S_v$ as high as 100 in order to illustrate fully the influence of viscous dissipation. However, as discussed previously, for practical electro-osmotically generated flows $S_v$ is of order 10 or less. For both geometries the qualitative behavior is similar. As $S_v \to 0$ viscous heating effects vanish, and the Nusselt number approaches values dependent only on $S$ and $Z$, as reported previously in a study neglecting viscous dissipation [37]. Indeed, the analysis reveals that for $S_v < 0.1$ the influence of viscous dissipation is negligible for all $S$ and $Z$. As $Z \to \infty$, the Nusselt number approaches the classical slug-flow results for both the circular tube and parallel plate channel ($Nu = 8$ and 12, respectively), regardless of the magnitudes of $S$ and $S_v$. At a sufficiently high value of $S_v$, the Nusselt number departs from the no-viscous-heating asymptote for all finite relative duct radii. The threshold value of $S_v$ at which departure occurs decreases for larger Joule heating (increasing $S$). Further,

the deviation from the $S_v \to 0$ condition is dependent on the relative duct ratio $Z$, and it occurs at slightly lower $S_v$ for the parallel plate channel than for the circular tube. Interestingly, for a given value of $S$, the magnitude of $S_v$ at which deviation from the no-viscous-heating asymptote is lowest for some intermediate value of $Z \approx 3$. This corresponds to the observed critical point in the $(E_v/E_e)/S_v$ vs. $Z$ distribution observed in Fig. 4.

The dependence of the fully-developed Nusselt number on the relative duct radius for two values of the dimensionless Joule heating parameter $S$, and the viscous heating parameter $S_v$ in the range 0.1–10 is shown in Figs. 7 and 8 for the circular tube and parallel plate channel, respectively. These values of dimensionless parameters are representative of what might be expected in typical electro-osmotic flows with finite wall heat flux. As noted previously, for $Z \to \infty$ (slug flow) the fully-developed Nusselt number approaches 8 and 12, respectively, for the circular tube and parallel plate channel at all values of $S$ and $S_v$. As $Z$ increases, although the velocity gradients increase significantly, the spatial region affected by viscous heating shrinks and vanishes in the limit as $Z \to \infty$. At low values of $Z$ the velocity profile mimics the classical Poiseuille flow, and the Nusselt number exhibits asymptotic behavior toward values that are dependent only on $S$. For this limiting case the results presented here approach those for a Poiseuille flow with uniform volumetric heating [42]. At these low values of $Z$ the wall-normal gradients of velocity are small, and viscous dissipation becomes important only for unrealistically large values of $S_v$ (e.g., unattainable electro-osmotically induced velocities). For sufficiently small $S_v$ the Nusselt number transition between the low-$Z$ and high-$Z$ asymptotic limits is monotonic. As noted previously, the influence of viscous dissipation is negligible for $S_v < 0.1$, and the Nusselt number's dependence on $S$ and $Z$ reproduces the results reported previously [37]. For $S_v > 0.1$ the Nusselt number deviates from this behavior at intermediate values of $Z$. This effect is more pronounced at increasing $S$ and $S_v$. There exists a local minimum in the Nusselt number's dependence on $Z$, where $Nu$ is lower than the low-$Z$ asymptotic value. This again corresponds to the relative duct radius at which viscous heating is most pronounced. This may be explained by the fact that in the absence of viscous heating the Nusselt number is seen to decrease with increasing Joule heating (increasing $S$) due to a rise in the wall temperature relative to the mixed mean temperature. Increases in $S_v$ represent additional, although non-uniformly spatially distributed, volumetric heating. Again, from a practical perspective, the results indicate that viscous heating will exercise influence on heat transfer principally in nanoscale channels, and for high Joule heating and large value of the viscous heating parameter $S_v$.

Fig. 9 shows local dimensionless temperature profiles in the circular tube for a relative duct ratio of $Z = 30$ for $S = 1$, 10, and 100 and $S_v = 0.1$, 1, and 10. The behavior for the parallel plate channel is qualitatively similar, and

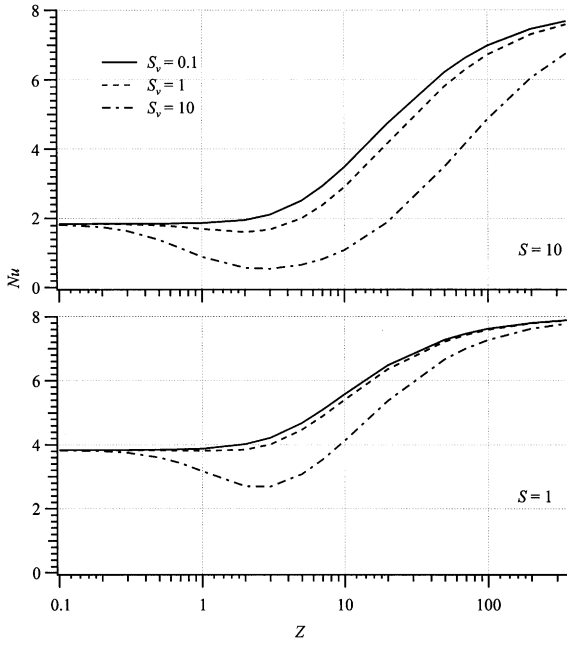


Fig. 7. Fully-developed Nusselt number in the circular tube with an imposed constant heat flux (fluid heating) plotted vs. $Z$ for $S = 1$ and 10, and $S_v = 0.1$, 1, and 10.

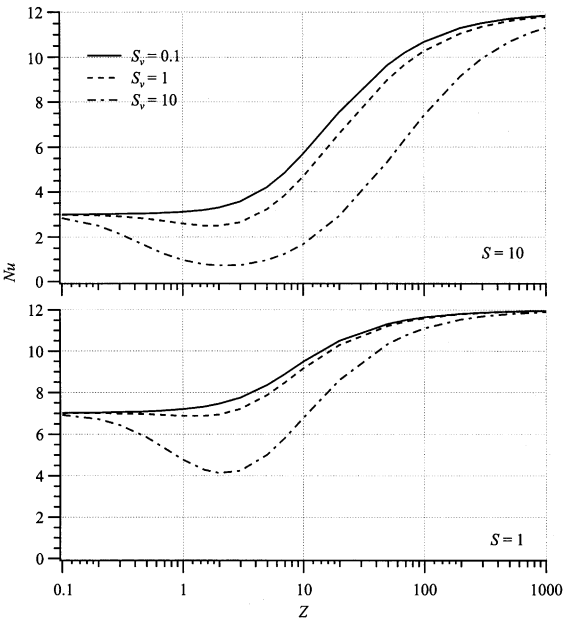


Fig. 8. Fully-developed Nusselt number in the parallel plate channel with an imposed constant heat flux (fluid heating) plotted vs. $Z$ for $S = 1$ and 10, and $S_v = 0.1$, 1, and 10.

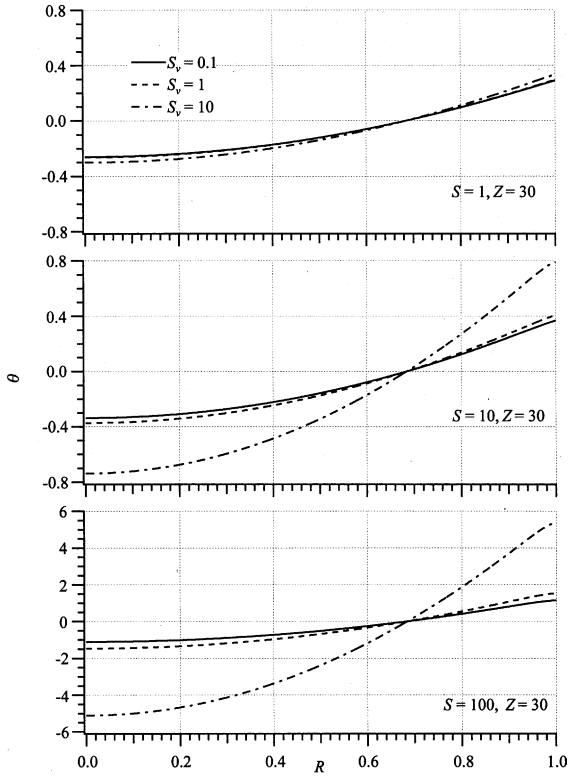


Fig. 9. Non-dimensional temperature distributions in the circular tube for $S = 1$, 10, and 100, $S_v = 0.1$, 1, and 10 and $Z = 30$. (Note the change of scale on the lower panel.)

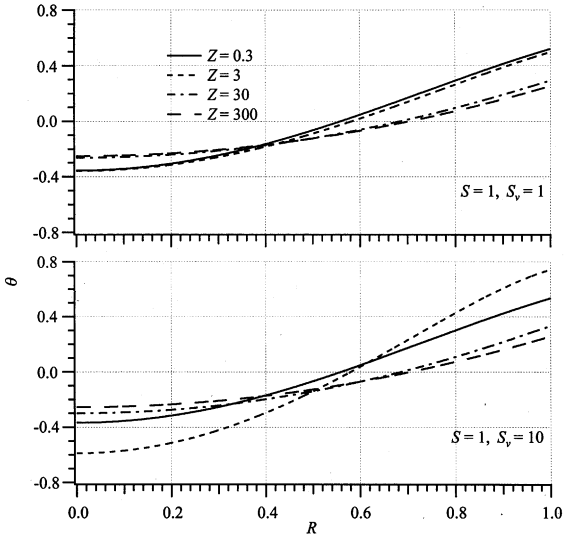


Fig. 10. Non-dimensional temperature distributions in the circular tube for $S = 1$, $S_v = 1$ and 10, and $Z = 0.3$, 3, 30, and 300.

is not shown here. For $S = 1$ the influence of viscous dissipation is entirely negligible for $S_v < 1$, and exercises little impact for $S_v$ as high as 10. There is greater variation in the local temperatures across the tube cross-section with increasing $S$ and $S_v$. Although the normalized wall temperature gradient is constant, $d\theta/dR|_{R=1} = 1$, the wall temperature increases both with increasing Joule heating ($S$) and viscous heating ($S_v$). The influence of viscous heating is most pronounced for the $S = 100$ and $S_v = 10$ case (bottom panel; note scale change). For such, the temperature variation across the channel can be significant.

The local dimensionless temperature is plotted in Fig. 10 for $S = 1$ for the relative duct radius in the range $0.3 \leqslant Z \leqslant 300$ and for $S_v = 1$ and 10. Again, results for the parallel plate channel are qualitatively similar. The upper panel illustrates that at $S_v = 1$ the temperature distributions for $Z = 0.3$ and 3 are quite similar, as are those for $Z = 30$ and 300. As was seen in the lower panel of Fig. 7 and discussed previously, the Nusselt number is approximately independent of $Z$ for $S = 1$ at the low- and high-magnitude extreme values of the relative duct radius. One would therefore expect very little change in the local temperature profile at the two extremes. For increasing viscous dissipation parameter ($S_v = 10$), only the $Z = 3$ case differs appreciably from the $S_v = 1$ profiles in the upper panel. This case now shows the largest variation in dimensionless temperature across the tube radius, with the highest wall temperature, resulting from the increased contribution of viscous heating at this relative duct radius.

## 5. Constant wall temperature

The differential equation governing thermal transport with uniform wall temperature is identical to that for the imposed constant wall heat flux, Eq. (9). However, the thermally fully-developed condition is stated $\partial T/\partial x = -\theta(dT_m/dx)$. For constant imposed wall temperature, the temperature field far downstream reaches an asymptotic condition where the temperatures cease to change, and therefore, $dT_m/dx = 0$. In this case, all energy generated volumetrically both by Joule and viscous heating is dissipated at the tube wall. Consequently, the imposed uniform wall temperature boundary condition yields a uniform wall heat flux, albeit negative with respect to direction (fluid cooling). Thus, retaining the same temperature normalization as in the constant wall flux condition is appropriate $[\theta = (T - T_m)/(q''_w a/k)]$, and the solution for the temperature distribution is

$$\theta - \theta_w = S[A_1(Y) - S_v A_3(Y, Z)] \tag{14}$$

The expressions for $A_1(Y)$ and $A_3(Y, Z)$ in Eq. (14) are identical to those for the constant wall heat flux solution, Eq. (12), found in Table 2. Indeed, the solution for $\theta - \theta_w$ (where $\theta_w$ is unknown, and must be determined

by evaluating the mixed mean temperature) in the constant wall temperature boundary condition is identical to the solution for the constant wall heat flux case with the exception that the numerator of the first term on the right-hand side of Eq. (12) vanishes. This term arises from the finite mean temperature gradient in Eq. (9). For the constant wall temperature boundary condition the asymptotic condition is $dT_m/dx = 0$, and all energy generated volumetrically by combined Joule and viscous heating is dissipated at the wall. Thus, an overall energy balance reveals that the total volumetric energy generation is dissipated by fluid convective cooling at the wall. For such a condition the energy balance yields the following relationship

$$S = -\frac{2^n}{1 + S_v F(Z)} \tag{15}$$

where $S$ and $S_v$ are defined as before for the constant wall heat flux boundary. Again, $n = 0$ and 1 for the parallel plate channel and circular tube, respectively, and the expression for $F(Z)$ is shown in Table 1 for both tube geometries. Note that for the constant wall temperature boundary condition $S$ and $S_v$ are not independent; a constant wall temperature condition is only possible for values of $S$ and $S_v$ which satisfy Eq. (15) for a given value of $Z$. Further, since the dimensionless Joule heating is defined as $S = s_e a/q''_w$, Eq. (15) confirms that for the constant wall temperature boundary condition (where the wall flux is negative due to fluid cooling), $S$ is always negative. Under constant wall temperature conditions Eq. (15) may be viewed as an indirect expression for the magnitude of the wall flux where the effects of both electro-osmotic Joule heating (for a given $s_e$) and viscous dissipation (for a given $\lambda$) are included. The dependence of $S$ on $S_v$ and $Z$ is shown in Fig. 11 for the two channel configurations studied. As may be seen, the asymptotic values for $S$ at vanishing $S_v$ (no influence of viscous heating) are $S = -1$ and $-2$ for the parallel plate channel and circular tube, respectively, as reported previously [37]. Fig. 11 reveals that for $S_v$ sufficiently large, $S$ deviates from the $S_v \to 0$ asymptote. The magnitude of $S_v$ at which departure from the low-$S_v$ limit is smallest for the critical value of relative duct radius, $Z \approx 3$, as observed in Fig. 4. At higher and lower values of $Z$ the departure occurs for larger $S_v$. Eq. (15) indicates that as $S_v \to \infty$, $S \to 0$ for any value of $Z$. However, recall that in practical electro-osmotic flows $S_v$ is of order 10 or less and thus, the effects of viscous heating are felt primarily for low values of the relative duct radius, and principally for $Z \approx 3$.

Substitution of Eq. (15) into Eq. (14) reveals that $\theta - \theta_w$ is independent of $S$, exhibiting dependence only on $S_v$ and $Z$. Correspondingly, the Nusselt number depends only on $S_v$ and $Z$. For the constant wall temperature condition, Fig. 12 illustrates the dependence of the

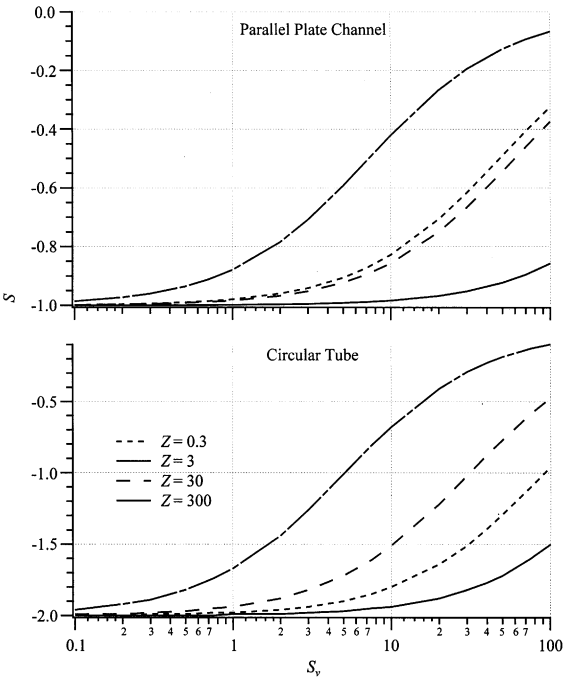


Fig. 11. Dependence of $S$ on $S_v$ necessary to maintain a constant wall temperature boundary for $Z = 0.3$, 3, 30, and 300.

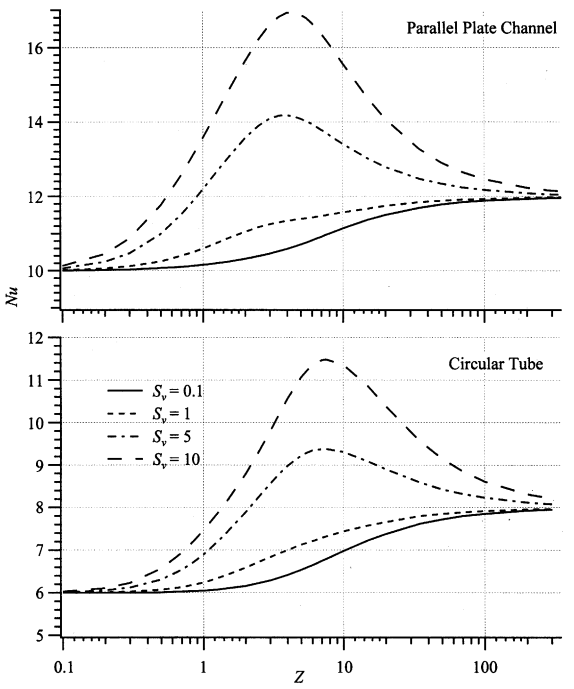


Fig. 12. Fully-developed Nusselt number for a constant wall temperature boundary condition (fluid cooling at a constant heat flux) plotted vs. $Z$ for $S_v = 0.1$, 1, 5, and 10, for the parallel plate channel and the circular tube.

Nusselt number on relative duct radius $Z$ for four values of $S_v$ for both channel geometries. In the limit as $Z \to \infty$, the Nusselt number approaches the classical slug-flow results independent of the magnitude of $S_v$, as described previously. The asymptotic limit for small $Z$ is the Nusselt number corresponding to a uniform wall temperature with fluid cooling at a constant (negative) wall flux, and is also independent of $S_v$. At low-$Z$ the velocity gradients are too low to generate appreciable viscous heating; at high-$Z$ where significant gradients occur, they are confined to vanishing area in the channel. In contrast to the results for the constant heat flux boundary condition with fluid heating, the Nusselt number *increases* for increasing $S_v$ at intermediate values of $Z$. This behavior reflects an increasing magnitude of the wall heat flux (for a fixed wall temperature, $T_w$) associated with higher viscous heating. Note that for $Z \approx 4$–7, a maximum in the Nusselt number exists for sufficiently high $S_v$. Contrast this behavior with the observed *minimum* Nusselt number in Fig. 10 for the case of fluid heating. At these intermediate values of $Z$ the Nusselt number may be significantly higher with viscous dissipation. For example, at $S_v = 10$ the maximum Nusselt number is approximately 80% higher than in the case of vanishing viscous heating. Interestingly, the maximum occurs at a relative duct radius somewhat greater than that corresponding to the minimum $Nu$ observed for the heat addition problem (Fig. 10).

## 6. Conclusions

The influence of viscous dissipation on thermally fully-developed, electro-osmotically generated convective transport has been analyzed for a parallel plate microchannel and circular microtube under imposed constant wall heat flux and constant wall temperature boundary conditions. For large ratio of the microtube radius (or microchannel half-width) to Debye length, the wall-normal fluid velocity gradients can be extremely high, which has the potential for significant viscous heating. The solution for the fully-developed, dimensionless temperature profile and corresponding Nusselt number have been determined for both geometries and for both boundary conditions. The problem is governed by three dimensionless parameters: the relative duct radius (ratio of the duct radius or plate gap half-width to Debye length), the dimensionless volumetric source (ratio of Joule heating to imposed wall heat flux), and a dimensionless parameter that relates the magnitude of the viscous heating to the Joule heating. This dimensionless parameter is dependent only on thermophysical and electro-osmotic properties of the fluid/channel combination; the parameter increases directly with fluid electrical resistivity, viscosity, and electro-osmotic mobility, and exhibits an inverse relation with the Debye length. It is shown that the influence of viscous dissipation is only important at large values of the dimensionless viscous heating parameter, and is significant only for low relative duct radii. For practical electro-osmotic flow/heat transfer applications, the effect of viscous heating on temperature distribution and Nusselt number is likely only for nanoscale channels. For such cases, viscous heating decreases the Nusselt number for the constant wall heat flux boundary condition (with fluid heating), and increases the Nusselt number for the constant wall temperature scenario.

## References

[1] P. Gravensen, J. Branebjerg, O.S. Jensen, Microfluidics—a review, J. Micromech. Microeng. 3 (1993) 168–182.
[2] S. Shoji, S. Nakagawa, M. Esashi, Micropump and sample injector for integrated chemical analysis systems, Sens. Actuators A 21 (1990) 189–192.
[3] B.H. van der Schoot, A. van den Berg, S. Jeanneret, N.F. de Rooij, A miniaturized chemical analysis system using two silicon micro pumps, in: Transducers '91, 1991, pp. 789–791.
[4] L. Bousse, C. Cohen, T. Nikiforov, A. Chow, A.R. Kopf-Sill, R. Dubrow, J.W. Parce, Electrokinetically controlled microfluidic analysis systems, Ann. Rev. Biophys. Biomol. Struct. 29 (2000) 155–181.
[5] Z. Shulin, Fabrication and characterization of electrokinetic micro-pumps, in: Thermomechanical Phenomena in Electronic Systems—Proceedings of the Intersociety Conference, vol. 2, 2000, pp. 31–36.
[6] C.T. Culbertson, R.S. Ramsey, J.M. Ramsey, Electro-osmotically induced hydraulic pumping on microchips: differential ion transport, Anal. Chem. 72 (2000) 2285–2291.
[7] P.K. Dasgupta, S. Liu, Electroosmosis: a reliable fluid propulsion system for flow injection analysis, Anal. Chem. 66 (1994) 1792–1798.
[8] N.A. Polson, M.A. Hayes, Electro-osmotic flow control of fluids on a capillary electrophoresis microdevice using an applied external voltage, Anal. Chem. 72 (2000) 1088–1092.
[9] S. Arulanandam, L. Dongqing, Liquid transport in rectangular microchannels by electro-osmotic pumping, Colloids Surf. A 161 (2000) 89–102.
[10] B.B. VanOrman, G.G. Liversidge, G.L. McIntire, Effects of buffer composition on electroosmotic flow in capillary electrophoresis, J. Microcolumn Sep. 2 (1990) 176–180.
[11] F.F. Reuss, Charge-induced flow, Proc. Imp. Soc. Natural. Moscow 3 (1809) 327–344.
[12] R.F. Probstein, Physicochemical Hydrodynamics, second ed., Wiley, New York, 1994.
[13] R.J. Yang, L.M. Fu, C.C. Hwang, Electroosmotic entry flow in a microchannel, J. Colloid Interface Sci. 244 (2001) 173–179.
[14] C.L. Rice, R. Whitehead, Electrokinetic flow in a narrow cylindrical capillary, J. Phys. Chem. 69 (1965) 4017–4024.
[15] D. Burgreen, F.R. Nakache, Electrokinetic flow in ultrafine capillary slits, J. Phys. Chem. 68 (1964) 1084–1091.

[16] S. Levine, J.R. Marriott, G. Neale, N. Epstein, Theory of electrokinetic flow in fine cylindrical capillaries at high zeta-potentials, J. Colloid Interface Sci. 52 (1974) 136–149.
[17] T.L. Sounart, J.C. Baygents, Electrically-driven fluid motion in channels with streamwise gradients of the electrical conductivity, Colloids Surf. A 195 (2001) 59–75.
[18] C. Yang, C.B. Ng, V. Chan, Transient analysis of electroosmotic flow in a slit microchannel, J. Colloid Interface Sci. 248 (2002) 524–527.
[19] S. Arulanandam, D. Li, Liquid transport in rectangular microchannels by electroosmotic pumping, Colloids Surf. 161 (2000) 29–102.
[20] L. Ren, D. Li, Electro-osmotic flow in hetrogeneous microchannels, J. Colloid Interface Sci. 243 (2001) 255–261.
[21] J.P. Gleeson, Electroosmotic flows with random zeta potential, J. Colloid Interface Sci. 249 (2002) 217–226.
[22] D.W. Arnold, P.H. Paul, Fluorescence-based visualization of electro-osmotic flow in microfabricated systems, in: Proceedings of SPIE—The International Society for Optical Engineering, Bellingham, WA, vol. 3877, 1999, pp. 174–179.
[23] P.H. Paul, M.G. Garguilo, D.J. Rakestraw, Imaging of pressure- and electrokinetically driven flows through open capillaries, Anal. Chem. 70 (1998) 2459–2467.
[24] J.A. Taylor, E.S. Yeung, Imaging of hydrodynamic and electrokinetic flow profiles in capillaries, Anal. Chem. 65 (1993) 2928–2932.
[25] D. Ross, T.J. Johnson, L.E. Locascio, Imaging of electro-osmotic flow in plastic microchannels, Anal. Chem. 73 (2001) 2509–2515.
[26] T. Tsuda, M. Ikedo, Observation of flow profiles in electroosmosis in a rectangular capillary, J. Chromatogr. 632 (1993) 201–207.
[27] E.B. Cummings, PIV measurement of electro-osmotic and pressure-driven flow components in microfluidic systems, in: Microelectromechanical Systems (MEMS), MEMS-Vol. 1, ASME, 1999, pp. 377–382.
[28] C. Yang, D. Li, J.H. Masliyah, Modeling forced liquid convection in rectangular microchannels with electrokinetic effects, Int. J. Heat Mass Transfer 41 (1998) 4229–4249.
[29] C. Yang, D. Li, Analysis of electrokinetic effects on the liquid flow in rectangular microchannels, Colloids Surf. 143 (1998) 339–353.
[30] G.M. Mala, D. Li, J.D. Dale, Heat transfer and fluid flow in microchannels, Int. J. Heat Mass Transfer 40 (1997) 3079–3088.
[31] L.N. Tao, The second fundamental problem in heat transfer of laminar forced convection, J. Appl. Mech. (June) (1962) 415–420.
[32] L.N. Tao, On some laminar forced-convection problems, ASME J. Heat Transfer 83 (1961) 466–472.
[33] W.A. Gobie, C.F. Ivory, Thermal model of capillary electrophoresis and a method for counteracting thermal band broadening, J. Chromatogr. 516 (1990) 191–210.
[34] J.H. Knox, Thermal effects and band spreading in capillary electro-separation, Chromatographia 26 (1988) 329–337.
[35] M.A. Bosse, P. Arce, Role of joule heating in dispersive mixing effects in electrophoretic cells: convective–diffusive transport aspects, Electrophoresis 21 (2000) 1026–1033.
[36] A.S. Rathore, K.J. Reynolds, L.A. Colon, Joule heating in packed capillaries used in capillary electrochromatography, Electrophoresis 23 (2002) 2918–2928.
[37] D. Maynes, B.W. Webb, Fully developed electro-osmotic heat transfer in microchannels, Int. J. Heat Mass Transfer 46 (2003) 1359–1369.
[38] D. Maynes, B.W. Webb, Fully-developed thermal transport in combined pressure and electro-osmotically driven flow in micro channels, in: Proceedings of the 6th ASME-JSME Thermal Engineering Joint Conference, Paper TED-AJ03-343, 2003.
[39] T.E. Valko, H. Siren, M. Riekkola, Characteristics of electro-osmotic flow in capillary electropheresis in water and in organic solvents without added ionic species, J. Microcolumn Sep. 11 (1999) 199–208.
[40] A.S. Rathore, E. Wen, C. Horvath, Electrosmotic mobility and conductivity in columns for capillary electrochromatography, Anal. Chem. 71 (1999) 2633–2641.
[41] L.C. Burmeister, Convective Heat Transfer, Wiley and Sons, New York, 1983.
[42] V.P. Tyagi, Laminar forced convection of a dissipative fluid in a channel, ASME J. Heat Transfer 88 (1966) 161–169.